Earth, Planets and Space

FULL PAPER Open Access

Recent eruption history inferred from eruption ages of the two latest lava flows using multi-dating at Yokodake Volcano, Japan

Hiroya Nitta[1,2*], Takeshi Saito[3] and Yorinao Shitaoka[4]

Abstract

Reconstruction of the eruption history of an active volcano is necessary to elucidate its volcanic activity and to assess the probability of its volcanic eruption. Yokodake volcano in central Japan is the only active volcano among the Yatsugatake volcano group. It has effused nine lava flows, most of which have not been dated. For this study, we ascertained the eruption ages of the latest lava (Y9) and second most recent lava (Y8) using radiocarbon (^{14}C), thermoluminescence (TL), and paleomagnetic dating methods. Results revealed the eruption ages of the two lava flows and the recent eruption history of Yokodake volcano. Yokodake volcano effused its Y8 lava flow at ca. 3.4 ka, ejected NYk-2 tephra with explosive eruption at ca. 2.4–2.2 ka, and effused the Y9 lava flow associated with Y9-T tephra at ca. 0.6 ka. Magma eruption rates of Yokodake at 34 ky and 3.4 ky were estimated as about 9×10^{-3} km^3/ky and 1×10^{-2} km^3/ky, indicating a stable eruption rate maintained during the past 34 ky. This result suggests that Yokodake volcano retains some potential for eruption, although the volcanic activity of the Yatsugatake volcanoes (10^{-1}–10^{-2} km^3/ky) has weakened over time.

Keywords: Eruption rate, Holocene lava, Paleomagnetic dating, Radiocarbon (^{14}C) dating, Thermoluminescence (TL) dating, Yatsugatake volcanoes

Introduction

Reconstruction of a volcano's eruption history is fundamentally important not only to elucidate its past volcanic activity, but also to prepare for future eruptions and to mitigate their damage. Understanding the latest activities of an active volcano in terms of their eruption styles, frequencies, and vent locations is particularly important for assessing risks of future volcanic activity. The radiocarbon (^{14}C) dating is frequently used for eruption age determinations of volcanic materials within the past few tens of thousands of years. Nevertheless, outlier dates can arise from the inclusion of contaminants such as mildew, mold, and fungus in samples, causing complicated interpretations of dating results. Moreover, it is often difficult to collect organic materials in volcanic contexts for ^{14}C dating.

Paleomagnetism can yield age indications directly from the eruptive materials. The volcanic material can acquire stable thermoremanent magnetization (TRM) during initial cooling from magmatic temperatures, which are usually higher than the Curie temperatures of magnetic minerals in the material. The eruption age of lava can be estimated (e.g., Alva-Valdivia et al. 2019; Pérez-Rodríguez et al. 2019; Risica et al. 2019) by comparing the paleosecular variation (PSV) curve with the paleodirection and paleointensity inferred from TRM. One inherent shortcoming of the method, however, is that the paleomagnetic age is not always uniquely identifiable because several candidates for age can be inferred from paleomagnetic data even if the paleodirection and paleointensity can be ascertained with high accuracy. Therefore,

*Correspondence: hiroya.nitta13@gmail.com
[2] Present Address: Kyushu Branch, Asia Air Survey Co., Ltd, 4-9-2 Hakata-ekimae, Hakata, Fukuoka 812-0011, Japan
Full list of author information is available at the end of the article

in most cases, paleomagnetic dating needs other dating techniques (Shitaoka et al. 2019).

Thermoluminescence (TL) dating, an alternative method for such direct dating, has been used widely for archaeological studies (Kondopoulou et al. 2015; Kharfi et al. 2019). Recently, TL method has been adopted to assess volcanic materials containing quartz or feldspar for age determination, thereby contributing to the establishment of detailed volcanic stratigraphic records (May et al. 2018; Sears et al. 2018).

Yokodake volcano is the only active volcano of the Yatsugatake volcano group in central Japan. Earlier geological studies revealed that the volcano was formed mainly as the result of nine lava flows, designated as Y1–Y9 (Kawachi 1974). The eruption ages of most flows have not been reported. The latest lava flow (Y9) is at the southern foot of the volcano. The second most recent (Y8) is at the eastern foot. Using ^{14}C dating, the eruption age of Y9 lava was estimated earlier as 2.35–2.15 cal ka BP (Okuno and Kobayashi 2010). However, that age was inferred not from the Y9 lava flow directly, but from NYk-2 tephra distributed at the Y9 lava flow periphery. Actual correlation of NYk-2 tephra to Y9 lava, therefore, remains ambiguous. For that reason, the eruption age of the Y9 lava flow merits re-examination. The Y8 lava age has not been determined, but the eruption of Y8 lava apparently occurred earlier than that of Y9 lava because the vegetation covering the Y8 lava was well developed and dense, whereas only poorly developed vegetation covered the Y9 lava.

Reconstruction of Yokodake volcanic activity is important not only for understanding the genesis and evolution of volcanic activity, but also for supporting more accurate prediction and characterization of its next likely activity. Because Yokodake has a ropeway operated year-round, the summit area has been a popular tourist destination, attracting about 300,000 people per year. That area includes the Y9 lava area. In fact, the summit ropeway station is located within 1 km of the expected crater region around the summit. The next volcanic disaster might be occurred even if the eruption is a small phreatic eruption as happened at Mt. Motoshirane of Kusatsu-Shirane volcano in 2018 (Ogawa et al. 2018).

As this report describes, we used ^{14}C, TL, and paleomagnetic methods to ascertain the eruption ages of the Y8 and Y9 lava flows for Yokodake volcano. Based on those results, we reconstructed its recent eruption history. Then, we discuss the eruption rate of Yokodake and present a comparison with the long-term eruption rate of other Yatsugatake volcanoes to evaluate the volcanic activity of Yokodake.

Geological setting

Geology of Yokodake volcano

The Yatsugatake volcanoes, which are located at the northern end of the Izu–Mariana arc, comprise a volcanic chain extending about 21 km along a NNW–SSE axis (e.g., Nishiki et al. 2007; Fig. 1). The volcanoes of this group can be subdivided into two sub-groups: the volcanoes south of the Natsuzawa Pass (southern Yatsugatake volcanoes) comprise several stratovolcanoes and lava domes of basalt and andesite, whereas the volcanoes north of the pass (northern Yatsugatake volcanoes) include stratovolcanoes consisting mainly of andesite and lava domes of rhyolite. The Yatsugatake volcanoes started their activity from about 0.5 Ma, but creation of most of the volcanic edifices occurred during ca. 0.4–0.2 Ma. Although the activity of the southern Yatsugatake volcanoes abated after 0.1 Ma, the northern Yatsugatake volcanoes have remained active (Nishiki et al. 2011). The total volumes of southern and northern Yatsugatake volcanoes have been estimated, respectively, as 102.4 km^3 and 37.6 km^3 (Nishiki et al. 2011).

Yokodake volcano (2480 m above sea level, 36° 5′ 14″ N, 138° 19′ 13″ E), located among the northern Yatsugatake volcanoes, is a Quaternary stratovolcano that has formed from nine lava flows (Y1–Y9; Kawachi 1974); it also has three volcaniclastic materials (Yt-Pm4 tephra, Oishi and Suzuki 2004; NYk-1 and NYk-2 tephra, Okuno 1995). Yokodake volcano consists of mostly andesites (58–63 wt% SiO_2) except for its Y1 rhyolitic lava flow (69.7 wt% SiO_2; Nakamura 1991). Although the onset age of the volcanic activity is unknown, the magmatic activity which produced Y9 lava flow occurred within the last 10,000 years. Therefore, Yokodake volcano is classified as an active volcano. The total volume of Yokodake volcano is estimated as ca. 1.1 km^3, as reported by Kawachi et al. (1978) and Oishi and Suzuki (2004).

Description of recent Yokodake ejecta

The Y8 lava, an andesite block lava flow at the eastern foot of the volcano, forms steep-sided mounds and ridges with thickness of at least 40 m. The lava block includes phenocrysts of plagioclase, orthopyroxene, clinopyroxene, Fe–Ti oxide, and hornblende; its groundmass crystallinity is high. The Y9 lava, an andesite block lava flow at the southeastern foot of the volcano, flows along the small valley with thickness of about 10–20 m. The lava block includes phenocrysts of plagioclase, orthopyroxene, and clinopyroxene, but phenocryst of Fe–Ti oxide is absent. The groundmass crystallinity is lower than that of

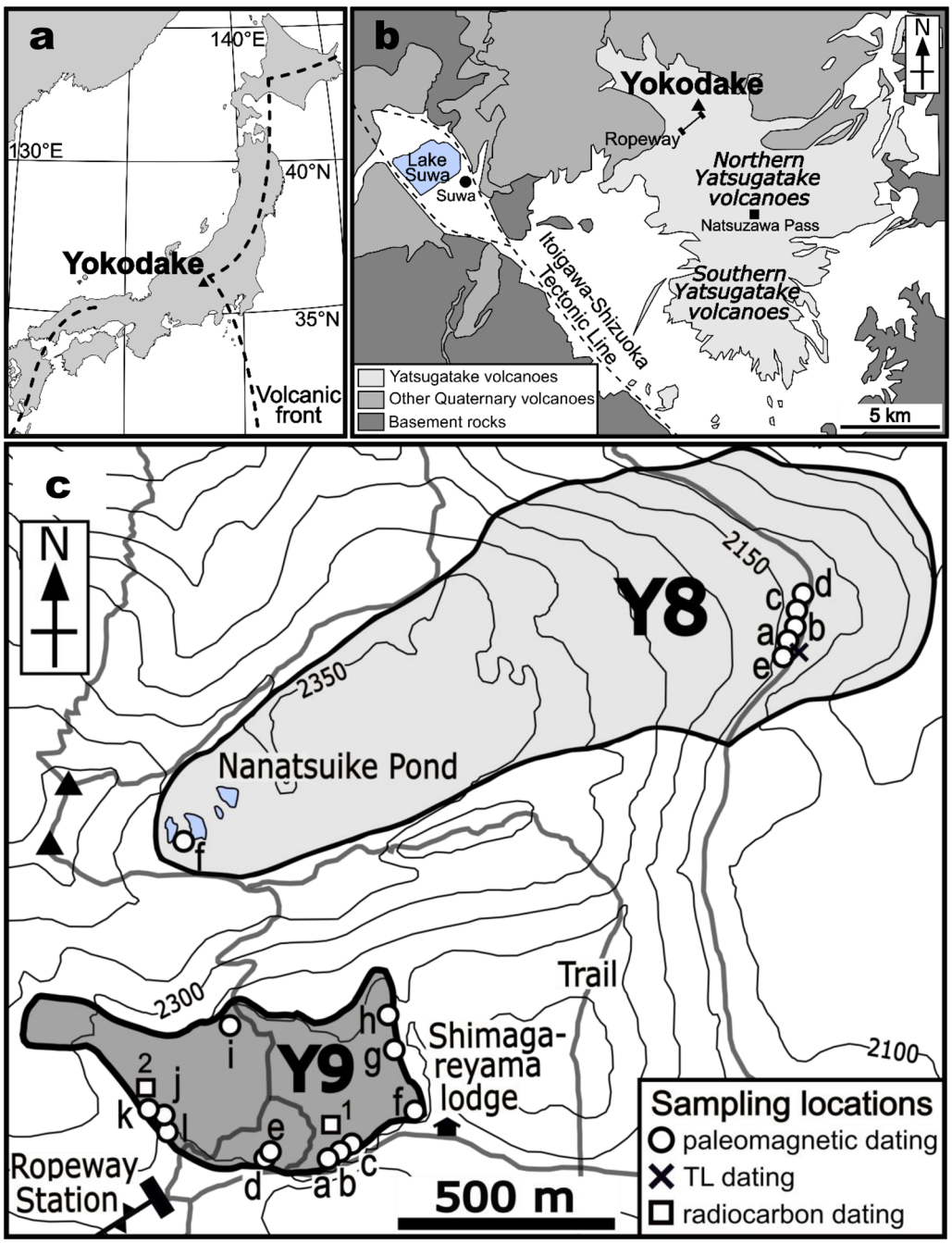

Fig. 1 **a** Index map of the Japanese islands showing Yokodake volcano. **b** Simplified geological map around Yatsugatake volcanoes referred from work by Nishiki et al. (2011). **c** Simplified geological map of the summit area of Yokodake volcano modified from that presented by Kawachi (1974). Distributions of Y8 and Y9 lava are shown. Circles, crosses, and squares, respectively, denote sampling locations for paleomagnetic dating, TL dating, and radiocarbon dating

the Y8 lava. The Y8 lava flow is covered by thick paleosol of more than about 30 cm, which supports well-developed vegetation, whereas most of the blocky lava surface of the Y9 lava flow remains exposed.

Around the volcano summit lies a fine-grained light-gray volcanic ash deposit with thickness of ca. 2–4 cm, hereinafter designated as the Y9-T tephra. Within the distribution of Y9 lava, Y9-T tephra directly cover Y9 lava. They are covered by paleosol of ca. 3–6 cm

thickness. The Y9-T tephra contains plagioclase, orthopyroxene, clinopyroxene, Fe–Ti oxide, hornblende, volcanic glass, lithic fragments, and altered fragments. Okuno (1995) reported light-gray fine-grained thin volcanic ash layer (NYk-1) that was distributed outside of the Y9 lava flow. From paleosol immediately below the NYk-1 tephra, its ^{14}C age estimated as ca. 0.9–0.7 ka. Okuno (1995) also reported volcanic ash deposits which apparently correlate to NYk-1 tephra were observed above the Y9 lava within the distribution of Y9 lava. However, he concluded that the deposits did not correlate to NYk-1 tephra because geological occurrence of the deposit was obscure as a tephra layer and ^{14}C age of paleosol immediately below the deposit was inferred as modern. Okuno and Kobayashi (2010) finally discarded NYk-1 tephra from Yokodake ejecta. The Y9-T tephra correlation with NYk-1 tephra is discussed later.

Underlying Y9-T tephra, a dark gray lapilli deposit with thickness of more than several tens of centimeters was identified around the summit. Although the deposit was observed above the Y8 lava, it was not found within the distribution of Y9 lava. It contains plagioclase, orthopyroxene, clinopyroxene, Fe–Ti oxide, hornblende, lithic fragments, and altered fragments. Lithic fragments are abundant. Volcanic glass is absent. These characteristics resemble those of NYk-2 tephra reported by Okuno (1995). Therefore, we correlate the deposit with NYk-2 tephra and call it as NYk-2, hereafter.

Eruption ages of volcanic materials from Yokodake

Information related to eruption ages of volcanic materials from Yokodake volcano is scarce. Among the 12 volcanic materials known to exist, only three tephra layers have been dated in earlier studies. The age of Yt-Pm4 tephra, which erupted between the Y5 and Y6 lava eruptions (Oba and Kawachi 1997), has been inferred from ^{14}C dating as 34 cal ka BP (Oishi 2015). Okuno (1995) reported the ^{14}C age for NYk-1 tephra, which first thought to be accompanied Y9 lava outflow, as ca. 0.9–0.7 ka. Okuno and Kobayashi (2010), however, revised the tephra accompanying the Y9 lava from NYk-1 to NYk-2 because NYk-1 did not show specific geological occurrence as a tephra layer and NYk-2 tephra seemed to be ejected from the crater located at the southern part of the summit, where Y9 lava flowed out. They inferred the eruptive age of Y9 lava, which is 2.35–2.15 cal ka BP, from the ^{14}C age found for NYk-2 tephra.

Methodology

Radiocarbon dating

At two localities, we collected paleosol samples just above Y9-T tephra (Fig. 1c). Using accelerator mass spectrometry (AMS), ^{14}C dating was conducted on request by the Institute of Accelerator Analysis Ltd., Kanagawa, Japan. Samples were cleaned chemically using acid treatment. The δ^{13}C obtained using the AMS were subsequently used to correct carbon isotopic fractionation when calculating conventional ^{14}C ages. Calibration to calendar years was based on IntCal13 using the ^{14}C calendar year calibration curve (Reimer et al. 2013) and a calibration program (OxCal v4.3; Bronk Ramsey 2009). We adopted two standard deviations (2σ) of calibrated ^{14}C age to evaluate the reliability of the results.

TL dating

We used rock samples of approximately 200 g from Y8 lava for this study (Fig. 1c). The surface layer of the rock sample, which had been exposed to sunlight, thereby reducing its luminescence, was removed using HF treatment. The sample was sieved using a crusher and standard sieves into a fraction of >50 μm, which was then crushed to fine silt (ca. 10–50 μm). The silt was then separated using Stokes' law of settling in acetone. The sieved sample was treated initially with 20% HCl for 90 min.

The TL measurement was performed using the original TL/OSL reader (NRL-99-OSTL2-KU; Shitaoka et al. 2015) at Rissho University. Samples were heated from 100 to 500 °C at a rate of 5 °C/s in a nitrogen atmosphere. The TL signal of 310–440 nm (FWHM) from a sample was guided to a photomultiplier tube (H7360-02; Hamamatsu Photonics KK) through two condensing lenses and optical filters (BG39; Schott AG and Corning 7-59; Hoya Corp.). Additive doses were administered using a small X-ray tube.

A standard multiple aliquot additive dose (MAAD) protocol (Aitken 1985) was applied to the treated sample. In the MAAD protocol, after TL was measured for both the natural sample and additive dose sample (artificially irradiated samples), the samples were divided into 11 fractions. Subsequently, some fractions were exposed to 6, 12, and 18 Gy at a dose rate of ca. 5 Gy/min. The equivalent dose (ED in Fig. 2) of the sample can be estimated by fitting the data assuming linear dose dependence. To correct the nonlinear portion in the low-dose region (Δ in Fig. 2), TL was measured using samples after the first glow measurement. Then ED and Δ were calculated by dividing the intercept by the slope.

The annual dose (dose rate) measurements were taken using a gamma-ray spectrometer. The U, Th, and K concentrations in the sample were analyzed using a Ge gamma-ray detector (7229P-7500S-2019; Canberra Japan K.K.). The annual dose was calculated using dose-rate conversion factors (Guérin et al. 2011; Rees-Jones 1995). Contributions of the cosmic dose rate to the annual dose

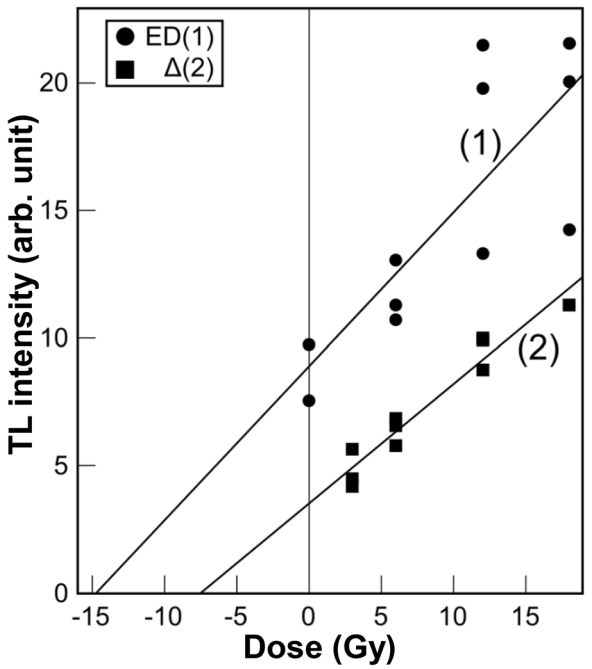

Fig. 2 TL growth curves for the equivalent dose (1) and nonlinear correction (2)

were assumed according to methods described in earlier reports by Prescott and Hutton (1994) and by Shitaoka et al. (2009).

Paleomagnetic dating

Paleomagnetic samples were collected from 18 outcrops for the Y8 and Y9 lava (Fig. 1c). Using a magnetic compass and, if possible, a sun compass, 59 lava samples were oriented. Specimens of 25 mm diameter and 22 mm height were cut from the oriented lava clasts at Shinshu University. The natural remanent magnetization (NRM) of each specimen was then measured using a spinner magnetometer (Re-Mag; Natsuhara-Giken). Specimens were demagnetized thermally using an electric furnace (TDS-1; Natsuhara-Giken). Progressive thermal demagnetization (PThD) was conducted up to 580–620 °C in air. Demagnetization results are shown on vector end-point diagrams (Zijderveld 1967). Using the diagrams, we determined the components of remanent magnetization and applied principal component analysis to each component (Kirschvink 1980). A stable magnetic component was defined as follows: (1) a linear segment consisting of more than three vector end points and (2) maximum angular deviation (MAD) of less than 10°. The mean direction of magnetization was calculated using Fisher statistics (Fisher 1953).

Paleointensity experiments were performed using 40 samples (Y8: 21, Y9: 19) that were selected based upon the PThD results. The samples had one stable magnetic component with little or no low-temperature magnetic component. Double heating IZZI-Thellier methods (Tauxe and Staudigel 2004; Yu et al. 2004) with pTRM checks (Coe 1967) were used. A field of 50 μT was applied during in-field heating treatments. Results of the experiments were analyzed using Arai plots (Nagata et al. 1963) with software (Thellier-Tool 4.22; Leonhardt et al. 2004). To assess the reliability of the results, we used ThellierTool A sets of selection criteria, as defined by Paterson et al. (2014).

Results

Radiocarbon dating

The ^{14}C ages of paleosols above Y9-T tephra obtained for samples from localities 1 and 2 were dated as 350 ± 20 yr BP and 510 ± 20 yr BP, which, respectively, correspond to calendar ^{14}C ages of 485–420 and 411–315 cal yr BP (2σ) (535–470 and 461–365 yrb2k) and to 550–510 cal yr BP (2σ) (600–560 yrb2k) (Table 1).

TL dating

The equivalent dose was estimated by extrapolation of the linear trend in diagrams of TL growth vs. dose. The temperature region of 415–425 °C satisfied the plateau test (Aitken 1985). The method for estimating nonlinearity correction was analogous to that of the equivalent dose (Fig. 2). The paleodose of the sample was calculated as the sum of the equivalent dose 14.7 ± 2.8 Gy and the nonlinear correction −6.8 ± 0.99 Gy. The annual dose was obtained as the sum of alpha, beta, gamma, and

Table 1 Results of radiocarbon dating

Sample	IAAA ID	Loc.	Material	Chemical pretreatment	^{14}C age (yr BP)	δ^{13}C (‰)	δ^{13}C-converted ^{14}C age (yr BP)	pMC (%)	Calendar ^{14}C age (cal yr BP) [probability (%)]	
18YK1-1	182379	1	Paleosol	HCL	330 ± 20	−24.13 ± 0.29	350 ± 20	95.77 ± 0.27	1σ	464–428 [27.9] 378–320 [40.3]
									2σ	485–420 [39.3] 411–315 [56.1]
18YK2-1	182380	2	Paleosol	HCL	500 ± 20	−24.35 ± 0.25	510 ± 20	93.79 ± 0.25	1σ	539–520 [68.2]
									2σ	550–510 [95.4]

Calibrated ages were calculated using Intcal13 (Reimer et al. 2013). We adopted the 2σ of calendar ^{14}C age

Table 2 Results of TL dating for Y8 lava

Paleodose (Gy)	U (ppm)	Th (ppm)	K (wt%)	Annual dose (mGy/a)	TL age (ka)
8.3 ± 2.97	1.09 ± 0.11	4.19 ± 0.54	1.20 ± 0.08	2.53 ± 0.28	3.3 ± 1.2

cosmic dose rates. The TL age divides the paleodose in the annual dose. The paleodose, annual dose, and TL age are presented in Table 2. The TL age of Y8 lava was obtained as 3.3 ± 1.2 ka.

Paleodirections

All specimens were found to have one or more stable magnetic components (Fig. 3). Four samples showed single magnetic components that decay linearly to the origin (Fig. 3a). Fifty-one samples included two components. Sixteen samples had a small low-temperature component for which the direction was distributed randomly (Fig. 3b). Therefore, we interpreted the high-temperature component as primary TRM, whereas the low-temperature component origin was inferred as secondary magnetization such as viscous remanent magnetization (VRM). Thirty-five samples showed a steadily low-temperature component that was separated sharply from the high-temperature component, for which the direction was well grouped (Fig. 3c). High-temperature components of these samples were scattered in direction, indicating that the lavas were adversely affected by a certain degree of rotation during or after lava emplacement. Low-temperature components acquired after emplacement of the lava were primary TRM in origin, with direction parallel to the geomagnetic field. Four samples comprised more than three components (Fig. 3d). The lowest-temperature components were well grouped. In these samples, low-temperature components probably originated from TRM acquired after emplacement.

The paleodirection of each sample was extracted using principal component analysis (Table 3). Most samples showed better grouping of the direction. The overall mean directions of Y8 and Y9 samples were Dec = 6.0°, Inc = 49.3°, α_{95} = 4.6°, k = 48.4, and Dec = 7.1°, Inc = 51.4°, α_{95} = 3.5°, k = 43.9. Some samples, however, showed a widely scattered direction, probably because of rotation during or after emplacement of the lava (Fig. 4). Using the outlier test of McFadden (1982), one sample for Y8 and three samples for Y9 were identified as outliers. They were ignored in calculations of the mean paleodirection. Consequently, mean paleodirections of Y8 (Dec = 5.1°, Inc = 50.6°, α_{95} = 3.9°, k = 70.0) and Y9 (Dec = 6.1°, Inc = 52.4°, α_{95} = 2.3°, k = 109.8) samples were obtained. The value of k in the Y8 results is not so good for young volcanic rocks. This scatter is probably attributable to failure to eliminate rotations during or after emplacement of the lava because most samples were obtained from the eastern slope of the lava (Fig. 1c). In addition, Y8 lava shows higher crystallinity than Y9 lava does. Y9 lava lacks phenocrysts of Fe–Ti oxide, indicating that the dominant grain size of magnetic mineral in Y8 samples is greater than that in Y9 samples. This might be another reason for the lower k value in Y8 results and might lead to the lower success rate of paleointensity experiments for Y8 lava, as discussed in "Paleointensities" section.

Paleointensities

Paleointensity experiments were conducted for 21 Y8 samples and 19 Y9 samples. Samples from which successful results were obtained showed linear decay in Arai plots (Fig. 5a, b). Some samples showed a straight line until moderate temperatures were reached, but the pTRM checks failed at high temperatures (Fig. 5c). Others had a low-temperature component that showed no linear decay, probably because of VRM (Fig. 5d). For these samples, paleointensities were calculated using data with straight decay. Some samples showed failure in pTRM checks and showed zigzag patterns or a nonlinear line throughout the experiments. They were rejected from consideration for paleointensity estimation (Fig. 5e, f). Consequently, 10 and 13 paleointensities were obtained, respectively, from Y8 and Y9 lava flows (Table 4). Success rates were 48% and 68% from Y8 and Y9 lava flow samples. The higher success rate of Y9 lava is probably attributed to the smaller dominant grain size of magnetic minerals in Y9 lava than that in Y8 lava. The estimated paleointensity values were well concentrated. Mean paleointensities of Y8 and Y9 lava were found to be 54.7 ± 2.8 and 54.0 ± 3.4 μT, which, respectively, correspond to virtual axial dipole moment (VADM) of $98.3 \pm 5.0 \times 10^{21}$ and $97.0 \pm 6.1 \times 10^{21}$ Am^2.

Discussion

Age determination of Y8 lava

The TL age of Y8 lava was inferred as 3.3 ± 1.2 ka, indicating the eruption age of Y8 lava as ca. 5.0 ka to 2.0 ka. However, the age might be older than the obtained TL value because of effects of anomalous fading of feldspar. Consequently, the paleomagnetic age was estimated by comparing our results to PSV data for the period of 7.0–2.0 ka. In this study, PSV data of paleointensity obtained from eastern Asia (Cai et al. 2017) were adopted because they represent the latest archaeointensity reference curve for eastern Asia combined with recently published data for Japan (Yu 2012), South Korea (Hong et al. 2013), and China (Cai et al. 2014, 2015). The paleointensity age was determined as a period in which each mean value of our data and PSV is shown within the error bars. As a result,

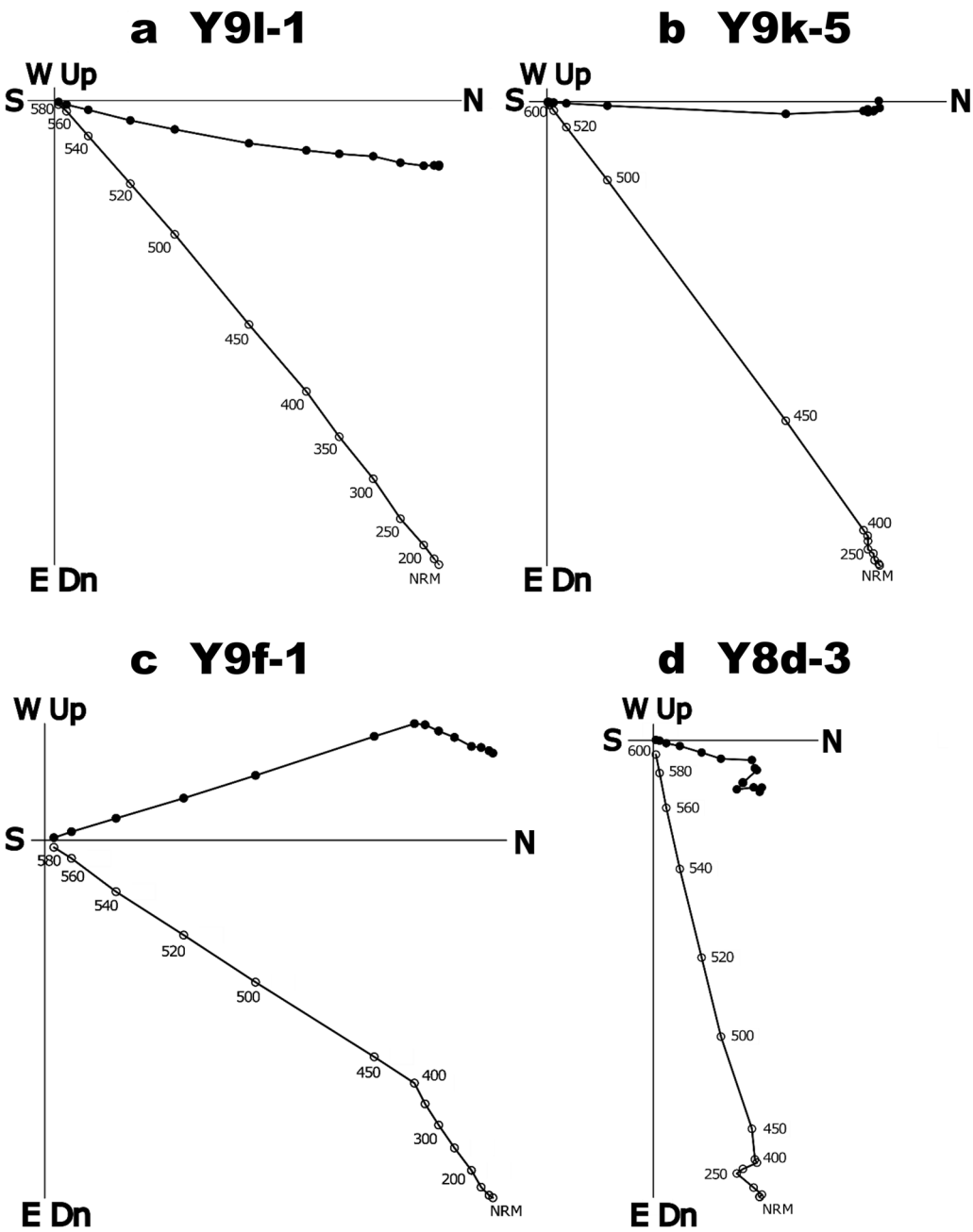

Fig. 3 Typical Zijderveld plots for PThD experiments. Solid and open circles, respectively, denote the horizontal and vertical projection. **a** One magnetic component with smooth decay to the origin. **b** Two magnetic components with a small low-temperature component. **c** Two magnetic components with a steady low-temperature component. **d** Multi-magnetic components

three periods were selected as paleointensity ages: ca. 3.75–3.50 ka, 3.45–3.20 ka, and 2.80–2.50 ka (Fig. 6d).

Based on paleointensity ages, the paleodirection result was compared to Holocene PSV data for 4.0–2.0 ka from Lake Biwa sediments (Ali et al. 1999) because Lake Biwa is geographically close to our study area and because the directional PSV has high temporal resolution for the past 10 ky. In comparison with PSV, the paleodirection of Y8 lava was recalculated as the values in Lake Biwa by

Table 3 Paleodirection results

Y8 lava		Paleodirections					Remark
Loc.	Sample	Dec (°)	Inc (°)	MAD (°)	*T* (°C)	Comp.	
a	1	19.8	46.4	0.7	400–600	2	
	2	14.7	50.2	1.1	500–600	2	
b	1	0.2	38.3	0.2	540–600	2	
	2	8.9	48.8	0.3	540–600	2	
c	1	30.7	54.4	1.6	150–250	2	
	2	19.4	54.1	1.9	100–200	2	
	3	16.4	44.7	4.3	100–350	2	
d	1	1.0	51.6	4.2	100–450	2	
	2	14.5	49.9	5.4	150–250	2	
	3	−4.5	40.0	1.6	150–250	>3	
	4	−15.6	40.7	7.9	100–300	2	
	5	8.9	55.6	5.4	100–400	2	
	6	0.0	56.6	7.8	100–300	2	
e	1	−8.3	58.9	0.6	400–620	2	
	2	−8.1	54.2	0.3	500–620	2	
	3	−7.9	51.6	0.3	500–620	2	
f	1	11.6	52.0	2.0	150–600	1	
	2	−6.5	55.1	2.2	350–600	2	
	3	12.8	45.1	3.6	200–300	2	
	4	18.0	20.7	1.1	100–600	1	*
	5	−4.0	51.8	1.4	150–600	1	

Mean	*n*/*N*	Dec (°)	Inc (°)	α_{95} (°)	*k*
1	21/21	6.0	49.3	4.6	48.4
2	20/21	5.1	50.6	3.9	70.0

Y9 lava		Paleodirections					Remark
Loc.	Sample	Dec (°)	Inc (°)	MAD (°)	*T* (°C)	Comp.	
a	1	19.6	47.4	5.8	100–400	2	
	2	−6.8	49.9	4.8	200–300	2	
	3	19.0	44.4	7.6	200–400	2	
b	1	13.1	39.9	5.8	150–250	2	
	2	8.3	21.0	6.3	150–250	2	*
	3	10.1	40.1	8.2	100–200	2	
c	1	18.1	49.2	2.7	150–250	2	
	2	11.5	59.9	9.1	100–350	2	
d	1	1.8	56.9	8.3	300–400	2	
	2	1.5	54.8	7.4	350–450	2	
	3	4.1	56.0	2.9	100–200	2	
e	1	−29.3	64.4	9.8	100–250	2	*
	2	31.2	61.6	9.2	100–200	>3	
	3	45.9	16.6	4.6	100–400	2	*
f	1	21.2	54.2	2.2	100–400	2	
	2	18.9	58.6	3.0	100–450	>3	
	3	−11.8	47.7	7.9	100–300	2	
g	1	−1.0	55.6	2.4	520–580	2	
	2	5.6	58.6	0.3	520–580	2	
h	1	−7.9	54.4	3.4	100–300	>3	
i	1	0.1	52.2	3.2	300–450	2	
	2	11.3	62.3	2.6	300–450	2	
	3	3.7	52.9	7.9	150–450	2	
j	1	5.3	55.5	7.1	100–400	2	
	2	7.2	50.9	5.8	150–250	2	
	3	4.0	47.0	8.1	100–250	2	
	4	0.9	48.7	4.6	250–350	2	
k	1	1.2	39.5	1.0	400–600	2	
	2	8.8	54.3	1.7	400–600	2	
	3	5.7	50.6	0.9	500–600	2	
	4	0.5	56.5	0.4	450–600	2	
	5	3.1	53.2	0.3	450–600	2	
	6	0.4	51.2	1.0	450–600	2	
l	1	10.3	49.6	0.9	100–580	1	
	2	4.5	52.4	4.2	200–400	2	
	3	2.4	54.3	4.5	250–450	2	
	4	−0.1	49.9	4.7	300–400	2	
	5	2.5	51.6	5.4	250–350	2	

Mean	*n*/*N*	Dec (°)	Inc(°)	α_{95}(°)	*k*
1	38/38	7.1	51.4	3.5	43.9
2	35/38	6.1	52.4	2.3	109.8

Dec, declination; Inc, inclination; MAD, maximum angular deviation; *T*, unblocking temperature range for the magnetic component from which paleodirection was obtained; Comp., number of magnetic components; *, rejected sample using the outlier test of McFadden (1982); *N*, total number of samples measured; *n*, number of samples used for calculation of the mean direction; α_{95}, 95% confidence angle; *k*, precision parameter; Mean 1, overall mean direction; Mean 2, mean direction of the accepted samples

assuming a geocentric dipole field. The paleodirection age was estimated as ca. 4.0–3.4 ka (Fig. 6a).

Combining the paleointensity age with the paleodirection age, two paleomagnetic ages of 3.75–3.50 ka and 3.45–3.40 ka were inferred (Fig. 7). Considering the mean value of the TL age (ca. 3.3 ka), the age of 3.45–3.40 ka is suitable as the eruption age. We conclude that the eruption age of Y8 lava is ca. 3.4 ka.

Age determination of Y9 lava

The ^{14}C ages of paleosols immediately above the Y9-T tephra indicate the eruption age of the Y9-T tephra as older than 0.55 cal ka BP. No soil layer exists between Y9-T tephra and Y9 lava, which indicates a lack of a long time interval between the two events. Petrographic features of Y9-T tephra resemble those of Y9 lava, and differ distinctively from those of Y8 lava and NYK-2 tephra: in fact, Y9 lava shows low crystallinity and Y9-T tephra contains volcanic glass. These findings suggest that Y9-T tephra and Y9 lava erupted, in geological terms, virtually

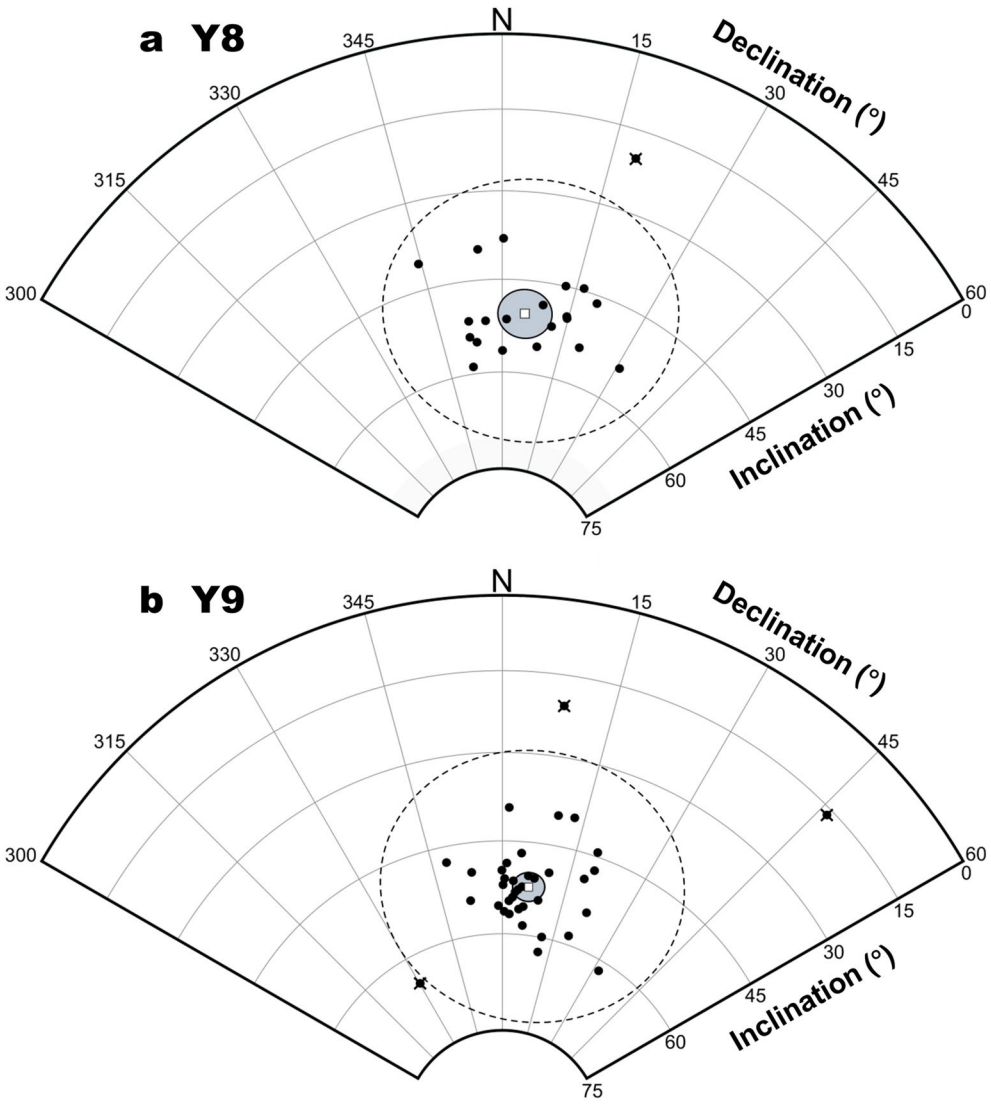

Fig. 4 Equal area projection of the paleodirection results for Y8 (**a**) and Y9 lava (**b**). Solid and open circles, respectively, represent projections onto the lower and upper hemisphere. The dashed circle is the rejection circle of McFadden (1982). Rejected results are denoted by crosses. Squares represent the mean direction with a 95% confidence circle, which is filled in as gray, after application of criteria by McFadden (1982)

simultaneously. Consequently, the eruption age of Y9 lava is older than 0.55 cal ka BP. In addition, thickness of the paleosol above the Y9-T tephra suggests that the paleosol of 3–6 cm can develop during 600 years, even in a snowy and windy mountain environment. This possibility implies that the eruption age of Y9 lava is not much greater than 0.55 cal ka BP. Consequently, the paleomagnetic age was estimated by comparing our results with PSV data during 1.6–0.6 ka.

The paleodirection obtained from the Japan Archeomagnetism Database (Hatakeyama and Shibuya 2012) was adopted as PSV because the database holds high-resolution PSV data established from archaeomagnetic data with high reliability. The PSV data were recalculated as the values in Yokodake by assuming a geocentric dipole field. Y9 lava coincides well with that of the paleodirection at ca. 0.60 ka: the latter is within the 95% confidence circle of the former (Fig. 6b). The PSV of eastern Asia in the last 1.6–0.6 ka (Cai et al. 2017) was adopted for paleointensity age estimation, as with Y8 lava. The VADM value from the PSV at ca. 0.60 ka is almost identical to that from Y9 lava (Fig. 6c). This age is consistent with ^{14}C results (Fig. 7). In fact, the eruption age is older than 0.55 cal ka BP, but it is not much older than 0.55 cal ka BP. We therefore conclude that the eruption age of Y9 lava is ca. 0.6 ka.

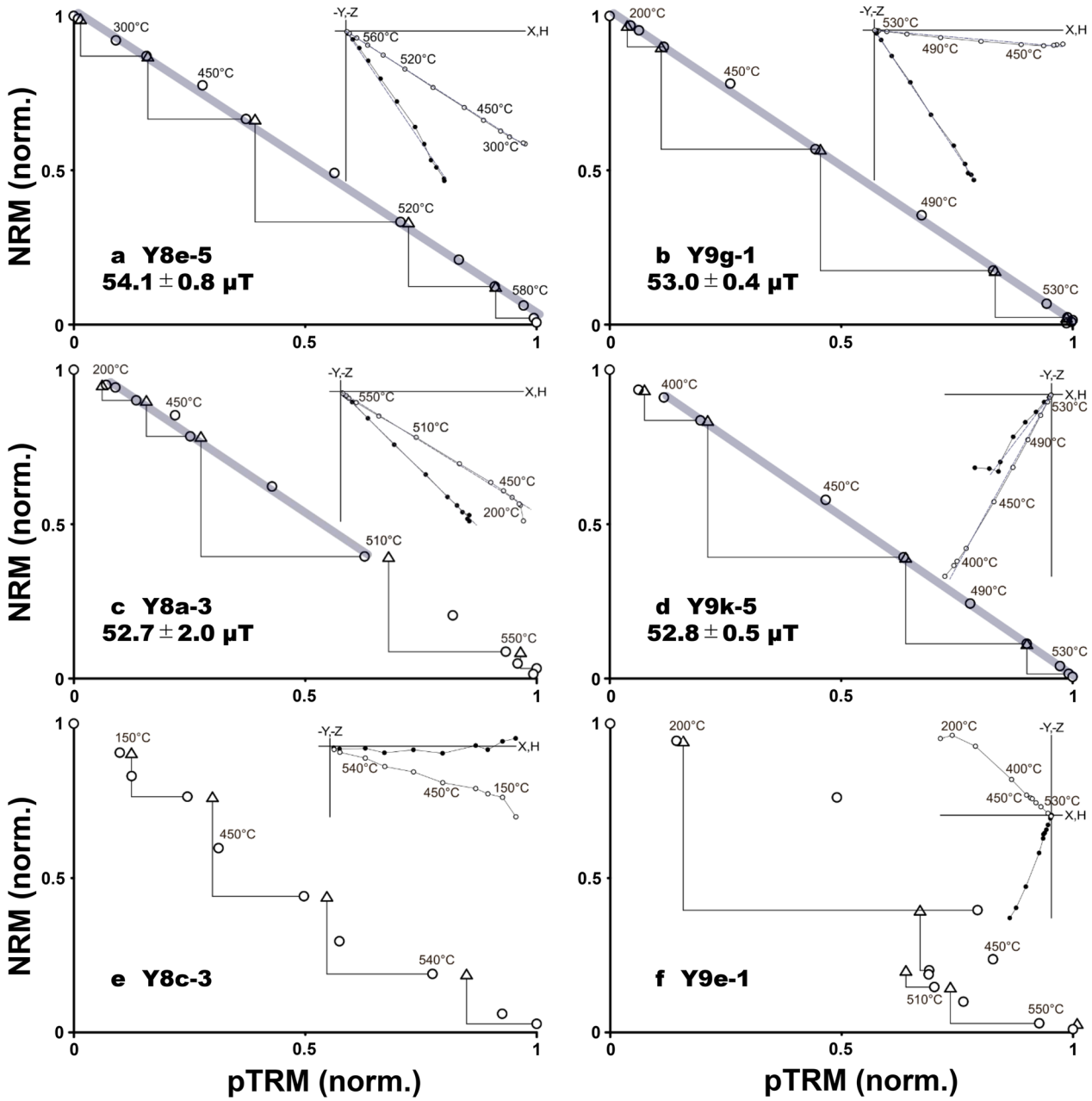

Fig. 5 Typical Arai plots of accepted (**a**–**d**) and rejected (**e**, **f**) specimens obtained from IZZI-Thellier experiments. Circles represent the normalized NRM vs. pTRM data with best-fit lines marked in gray. pTRM checks are shown as triangles. Zijderveld plots of the experiments are also shown as inset figures. Paleointensity analysis was conducted using ThellierTool (Leonhardt et al. 2004)

Correlation of tephra layers and consistency of the estimated ages

Our results indicate that the eruption ages of Y8 and Y9 lava are, respectively, ca. 3.4 ka and 0.6 ka. The Y8 age is a new result. The Y9 age is about 1.8–1.6 ky younger than values reported from earlier works (NYk-2 tephra, 2.4–2.2 ka) by Okuno and Kobayashi (2010). The Y9 age is also approximately equal to the age of NYk-1 tephra (0.9–0.7 ka) reported by Okuno (1995). It is suggested that Y9-T tephra, which accompanied the effusion of Y9 lava, correlates to NYk-1 tephra. The ^{14}C age of 0.9–0.7 ka was slightly older than our value of 0.6 ka. It probably indicated that there is small age gap between the tephra and

Table 4 Paleointensity results

Sample	*T* (°C)	*N*	*β*	*f*	*q*	MAD_{anc} (°)	*α* (°)	δCK (%)	δpal (%)	PI ± *σ* (μT)
Selection criteria		≥ 5	≤ 0.1	≥ 0.35	≥ 5	≤ 6	≤ 15	≤ 7	≤ 10	
Y8 lava										
a-3	200–510	7	0.04	0.54	10.33	0.55	0.64	2.16	9.26	52.7 ± 2.0
a-4	400–580	7	0.02	0.69	28.85	1.63	2.02	2.06	2.80	60.4 ± 1.2
c-1	0–580	11	0.02	0.91	38.79	0.82	0.75	1.99	4.85	49.6 ± 1.0
c-5	0–580	11	0.02	0.88	42.21	1.15	1.54	3.68	9.96	54.9 ± 1.0
d-1	0–510	8	0.05	0.35	5.26	0.74	1.95	1.49	7.70	54.4 ± 2.9
e-1	150–580	9	0.02	0.90	47.74	0.93	0.99	2.10	1.32	55.5 ± 0.9
e-4	200–500	6	0.04	0.58	10.68	0.66	1.06	4.75	9.95	53.6 ± 2.2
e-5	0–600	12	0.01	0.96	60.99	0.89	0.76	1.88	4.97	54.1 ± 0.8
e-6	0–520	8	0.02	0.55	19.00	0.92	2.39	2.40	9.90	54.4 ± 1.3
e-8	200–520	7	0.05	0.56	9.83	0.72	1.16	2.90	9.65	57.0 ± 2.6
Mean										54.7 ± 2.8
Y9 lava										
d-2	250–580	10	0.01	0.90	111.27	1.41	1.10	3.96	9.75	49.4 ± 0.3
e-3	400–550	8	0.02	0.78	25.84	0.60	0.50	1.32	2.23	61.0 ± 1.5
g-1	0–590	12	0.01	0.98	101.24	0.76	0.36	1.07	0.61	53.0 ± 0.4
i-2	100–560	11	0.02	0.94	41.00	0.83	0.71	1.22	4.45	58.4 ± 1.1
i-3	0–580	11	0.02	0.98	41.15	0.52	0.33	2.57	6.31	53.2 ± 1.1
i-4	0–400	6	0.02	0.81	13.82	1.26	1.46	0.52	0.10	53.7 ± 1.2
i-5	0–580	11	0.01	0.97	60.27	0.90	0.59	2.90	7.19	52.6 ± 0.7
j-4	200–580	10	0.01	0.95	70.51	0.54	0.36	3.21	0.68	57.5 ± 0.6
k-2	400–580	9	0.01	0.88	144.84	1.16	0.71	3.38	8.38	51.2 ± 0.3
k-4	0–580	11	0.01	0.97	61.42	0.42	0.09	3.11	1.41	55.4 ± 0.7
k-5	400–580	9	0.01	0.87	79.32	1.60	0.60	1.54	1.54	52.8 ± 0.5
k-6	400–580	9	0.01	0.90	65.27	0.75	0.46	4.31	0.37	54.2 ± 0.6
l-4	400–590	9	0.01	0.88	80.48	0.47	0.24	4.75	9.25	49.3 ± 0.4
Mean										54.0 ± 3.4

Selection criteria are listed in the first row. *T*, temperature used to ascertain the paleointensity; *N*, number of points included in the linear best-fit; *β*, ratio of standard error of the slope of the selected segment in the Arai plot to the absolute value of the slope; *f*, fraction of the NRM used for best-fit; *q*, quality factor; MADanc, anchored maximum angular deviation; *α*, angular difference between anchored and non-anchored best solution; δCK, relative check error; δpal, cumulative check difference; PI ± *σ*, paleointensity and standard deviation

the ^{14}C sample, although it was obtained from immediately below the tephra layer, whereas the value found in the present study was based upon the paleomagnetic age obtained directly from the lava.

The petrographic features and the distribution of the tephras both indicate that Y9-T tephra correlates not to NYk-2 tephra but to NYk-1 tephra. Whereas NYk-2 tephra comprises coarse thick lapilli layers characterized by abundant lithic fragments and lack of volcanic glass, Y9-T tephra and NYk-1 tephra are light-gray fine-grained thin volcanic ash layers containing volcanic glass. Also, Y9 lava shows low crystallinity. These findings collectively suggest that Y9-T tephra is identical to NYk-1 tephra. Within the distribution of Y9 lava, Y9-T tephra can be observed above the Y9 lava, but NYk-2 tephra can not be similarly observed. Furthermore, NYk-2 tephra is distributed outside of the Y9 lava flow. Our results revealed that Y9 lava was effused about 1.8–1.6 ky after the NYk-2 tephra eruption. Consequently, the tephra was covered by Y9 lava within the distribution of Y9 lava, which led to the absence of the tephra layer above Y9 lava.

In addition, our results were consistent with the differing development of vegetation found above the two lava flows. The thin paleosol of about 3–6 cm found above Y9 lava is consistent with sparse vegetation, whereas the thick paleosol of more than about 30 cm accumulated during about 3000 years above Y8 lava is capable of supporting well-developed vegetation. The average sedimentation rates of paleosol above both lava flows are estimated as similar values of ca. 9 cm/ky for Y8 and 5–10 cm/ky for Y9. These values are nearly equal to the average sedimentation rate of paleosol in Japan (10 cm/ky; Hayakawa 1995).

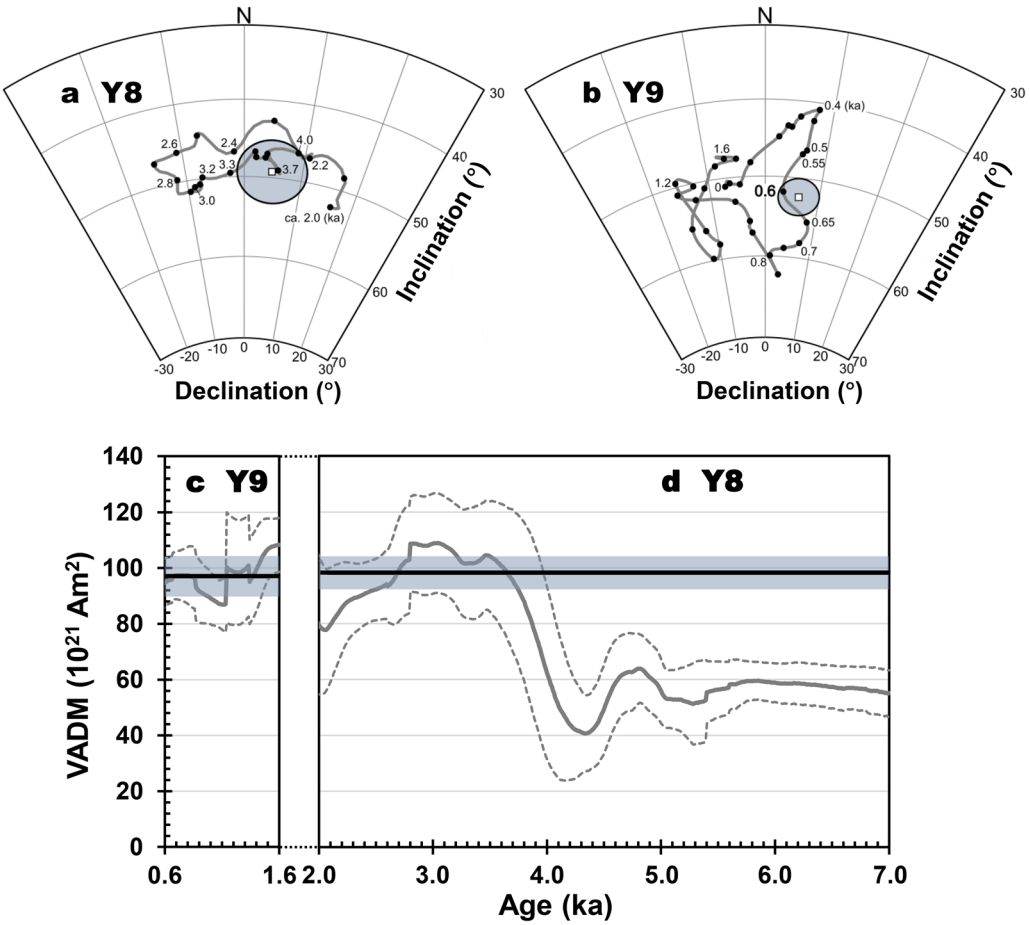

Fig. 6 PSV record during the past 4.0–2.0 ka (**a**) and 7.0–2.0 ka (**d**) for Y8 lava and 1.6–0.6 ka for Y9 lava (**b**, **c**) and our paleomagnetic results. Paleodirection obtained from Lake Biwa sediments (Ali et al. 1999) and that from the Japan Archeomagnetism Database (Hatakeyama and Shibuya 2012) were adopted, respectively, as PSV to paleodirection age estimation for Y8 (**a**) and Y9 (**b**) lava. Paleointensity data obtained from eastern Asia (Cai et al. 2017) were adopted as PSV for paleointensity age estimation (**c**, **d**). Mean paleodirections of Y8 (**a**) and Y9 (**b**) lava and their 95% confidence angles are shown, respectively, as open squares and gray circles. Estimated VADM values of Y9 (**c**) and Y8 (**d**) lava and their standard deviations are shown, respectively, as bold lines and gray bars

We conclude that Y9-T tephra correlates with NYk-1 tephra and that Yokodake erupted three times after the Y8 eruption inclusive: Y8 lava was effused at ca. 3.4 ka. NYk-2 tephra was ejected at ca. 2.4–2.2 ka. The latest eruption at ca. 0.6 ka produced Y9 lava and Y9-T tephra.

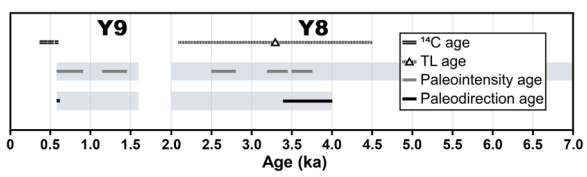

Fig. 7 Comparison of ^{14}C, TL, paleodirection, and paleointensity age results. ^{14}C ages are shown as years before AD 2000 (yrb2k) (2σ). Mean value of TL age (3.3 ka) is denoted by open triangles. Time ranges in which paleomagnetic datings were carried out were marked in gray

Eruption rate

The magma eruption rate of Yokodake volcano was estimated based upon our results and upon earlier data related to age and volume. Five lava flows (Y1–Y5; Kawachi 1974) that occurred at the early stage of the volcano have not been dated. In fact, Yt-Pm4 tephra is the oldest volcanic material for which the age has been estimated. Therefore, the eruption rate after the ejection of Yt-Pm4 tephra can be discussed. The estimated age, volume, and eruption rate are presented in Table 5. The dense rock equivalent (DRE) volume and age of Yt-Pm4

Table 5 Age and volume of eruptive products and estimated eruption rate of Yokodake during the last 34 ky and 3.4 ky

Unit	Age (ka)	Volume (DRE, km^3)	Span (ky)	Eruption rate (km^3/ky)
Y9-T tephra	0.6	5×10^{-4}		
Y9 lava	0.6	3×10^{-3} [a]		
NYk-2 tephra	2.4–2.2[b]	8×10^{-4}		
Y8 lava	3.4	3×10^{-2} [a]		
Total 1		3.4×10^{-2}	3.4	1.0×10^{-2}
Y7 lava	N.D.	4×10^{-2} [a]		
Y6 lava	N.D.	3×10^{-2} [a]		
Yt-Pm4 tephra	34[c]	2×10^{-1} [d]		
Total 2		3.04×10^{-1}	34	9.0×10^{-3}

DRE volumes of tephras were calculated by assuming deposit density of 1.0 g/cm^3 and dense rock density of 2.5 g/cm^3. Eruption rates during the last 3.4 ky (Total 1) and 34 ky (Total 2) were estimated. N.D. signifies no data available

Data were referred from the following sources: [a] Kawachi et al. (1978), [b] Okuno and Kobayashi (2010), [c] Oishi (2015), [d] Oishi and Suzuki (2004)

tephra were estimated, respectively, as about 0.2 km^3 (Oishi and Suzuki 2004) and 34 ka (Oishi 2015). After the Yt-Pm4 tephra eruption, four lava flows (Y6–Y9) were effused (Oba and Kawachi 1997). The volumes of Y6, Y7, Y8, and Y9 lava were estimated, respectively, as about 0.03, 0.04, 0.03, and 0.003 km^3 (Kawachi et al. 1978). The eruption ages of Y8 and Y9 lava were estimated as about 3.4 ka and 0.6 ka from the present study, whereas Y6 and Y7 lava did not date. The DRE volumes of NYk-2 and Y9-T tephra were estimated as about 8×10^{-4} km^3 and 5×10^{-4} km^3, respectively, assuming linear change of the deposit thickness and a simple cone shape.

The magma eruption rate of Yokodake after ejection of Yt-Pm4 tephra was estimated for the past 34 ky as about 9×10^{-3} km^3/ky (Fig. 8). The eruption rate after the effusion of Y8 lava for the past 3.4 ky was estimated as about 1×10^{-2} km^3/ky, which is similar to the rate estimated for the past 34 ky. The long-term eruption rates of Yatsugatake volcanoes and northern Yatsugatake volcanoes were estimated, respectively, as about 2.8×10^{-1} km^3/ky and 7.5×10^{-2} km^3/ky using the values of ages and volumes estimated by Nishiki et al. (2011) (Fig. 8b).

The long-term eruption rates of Yatsugatake volcanoes are comparable to those of other active volcanoes in Japan: the average eruption rates of active volcanoes in Japan were estimated as about 0.1–1 km^3/ky (Ono 1990). The eruption rate of Yokodake is about one order of magnitude lower than that of the entire volcano group, suggesting that the volcanic activity of Yatsugatake volcanoes became weaker. This result is consistent with the shrinking active region at Yatsugatake volcanoes during

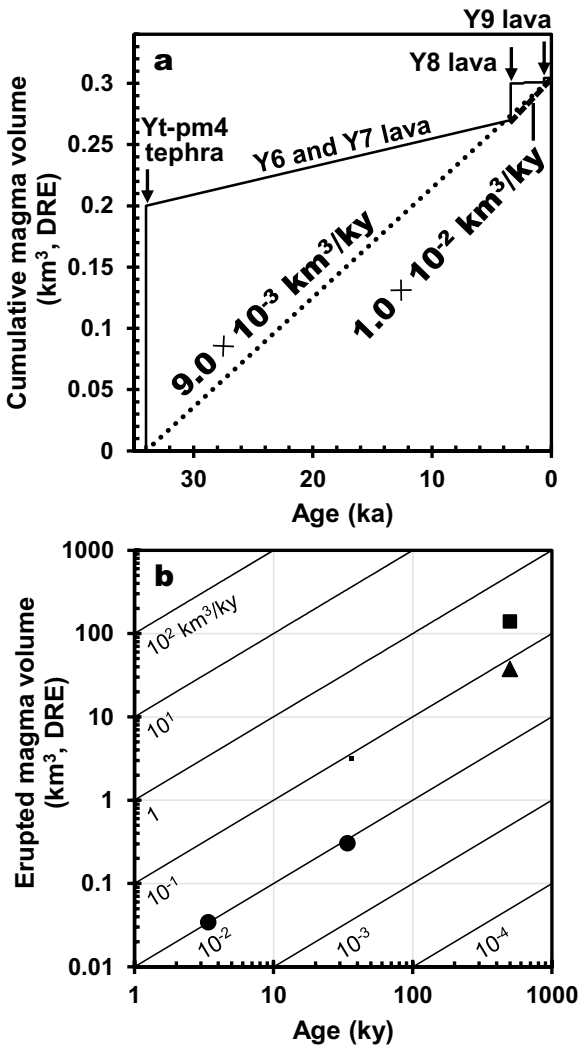

Fig. 8 **a** Cumulative magma volume derived from Yokodake volcano. Dotted and dashed lines, respectively, indicate the eruption rate at 34 ky and 3.4 ky. **b** Estimated magma eruption rate of Yokodake volcano, northern Yatsugatake, and all Yatsugatake volcanoes obtained using our data and earlier results (Kawachi et al. 1978; Oishi and Suzuki 2004; Okuno and Kobayashi 2010; Nishiki et al. 2011; Oishi 2015). Circles represent the eruption rate of Yokodake during the past 34 ky and 3.4 ky. The triangle and square, respectively, represent the eruption rates of northern Yatsugatake and Yatsugatake volcanoes during a 0.5-My period

the past 0.5 Ma. Their peak of activity occurred during ca. 0.4–0.2 Ma. Southern Yatsugatake volcanoes became calm after 0.1 Ma; only Yokodake volcano has remained active in the Holocene (Nishiki et al. 2011). Although the volcanic activity of all Yatsugatake volcanoes has weakened over time, our results indicate that the eruption rate of Yokodake volcano has not declined during the past 34 ky, suggesting that the volcanic activity of Yokodake

might continue for some time into the future with an eruption rate of about 10^{-2} km^3/ky.

Conclusions

The recent eruption history of Yokodake volcano was elucidated using multiple dating techniques, with application of ^{14}C, TL, and paleomagnetic methods to the two most recent lava flows (Y8 and Y9) of the volcano. Results have yielded volcanic activity estimates as presented below. The Y8 lava flow distributed at the eastern foot of the volcano was effused at ca. 3.4 ka. Explosive eruption without lava effusion occurred at ca. 2.4–2.2 ka, which led to ejection of NYk-2 tephra. The last activity, which occurred at ca. 0.6 ka, led to development of Y9 lava flows on the southern slope of the volcano, which were associated with Y9-T tephra. Magma eruption rates of Yokodake in 34 ky and 3.4 ky were estimated, respectively, as about 9×10^{-3} km^3/ky and 1×10^{-2} km^3/ky. Recent eruption rates are about one order of magnitude lower than the long-term eruption rates of the Yatsugatake volcano group (10^{-1}–10^{-2} km^3/ky), suggesting a decrease of the volcanic activity of the entire Yatsugatake volcano group. Recent eruption rates during two periods have been estimated as approximately equal values of about 10^{-2} km^3/ky. Volcanic activity at Yokodake might continue for some time into the future, although the eruption rate is not high. This study demonstrated the use of multiple methods of dating as an effective tool for determining the age of young volcanic deposits. The reconstructed eruption history of Yokodake volcano is more active than that reported earlier. Substantial lava effusion at ca. 0.6 ka indicates that Yokodake is not an active volcano with low activity. It retains some potential for eruption, thereby spurring our recommendation that preventive measures against volcanic disasters be modified and reinforced at Yokodake, as it is a very popular tourist destination.

Abbreviations

TL: Thermoluminescence; TRM: Thermoremanent magnetization; PSV: Paleosecular variation; AMS: Accelerator mass spectrometry; MAAD: Multiple aliquot additive dose; ED: Equivalent dose; NRM: Natural remanent magnetization; PThD: Progressive thermal demagnetization; MAD: Maximum angular deviation; VRM: Viscous remanent magnetization; VADM: Virtual axial dipole moment; DRE: Dense rock equivalent.

Acknowledgements

We would like to thank Dr. A. Hayashida and Dr. T. Hatakeyama for advice related to the PSV data of paleodirection. Dr. Y. Yamamoto is acknowledged for advice about paleointensity age determination. Helpful suggestions about statistics of paleomagnetic data from Dr. N. Ishikawa are appreciated. The authors thank Dr. T. Oikawa for geological advice and suggestions. This study was conducted under the cooperative research program of Research Institute for Natural Hazards and Disaster Recovery, Niigata University (2018–19; PI, TS) and JSPS KAKENHI Grant number 16H01826 to TS. HN was supported by the MEXT Integrated Program for Next Generation Volcano Research and Human Resource Development. The authors appreciate and acknowledge Dr. Yongjae Yu, Dr. Chuang Xuan and Dr. H. Shibuya for their thoughtful reading and constructive comments, which have greatly improved the manuscript.

Authors' contributions

HN conducted geological surveys and paleomagnetic experiments under the supervision of TS. YS took TL measurements and compiled and interpreted the TL results. HN compiled and interpreted all data and composed the manuscript with help from TS. All authors read and approved the final manuscript.

Funding

This study was conducted under the cooperative research program of the Research Institute for Natural Hazards and Disaster Recovery, Niigata University (2018–19; PI, TS) and JSPS KAKENHI Grant number 16H01826 to TS. HN was supported by the MEXT Integrated Program for Next Generation Volcano Research and Human Resource Development.

Availability of data and materials

The datasets used and analyzed for the current study are available from the corresponding author on reasonable request.

Competing interests

The authors declare that they have no competing interests.

Author details

[1] Graduate School of Science and Technology, Shinshu University, 3-1-1 Asahi, Matsumoto, Nagano 390-8621, Japan. [2] Present Address: Kyushu Branch, Asia Air Survey Co., Ltd, 4-9-2 Hakata-ekimae, Hakata, Fukuoka 812-0011, Japan. [3] Institute of Science, Academic Assembly School of Science and Technology, Shinshu University, 3-1-1 Asahi, Matsumoto, Nagano 390-8621, Japan. [4] Department of Environment System, Faculty of Geo-environmental Science, Rissho University, 1700 Magechi, Kumagaya, Saitama 360-0194, Japan.

Received: 27 December 2019 Accepted: 23 June 2020
Published online: 16 July 2020

References

Aitken MJ (1985) Thermoluminescence dating. Academic Press, London, p 359
Ali M, Oda H, Hayashida A, Takemura K, Torii M (1999) Holocene paleomagnetic secular variation at Lake Biwa, central Japan. Geophys J Int 136:218–228
Alva-Valdivia LM, Rodríguez-Trejob A, Moralesc J, González-Rangela JA, Agarwal A (2019) Paleomagnetism and age constraints of historical lava flows from the El Jorullo volcano, Michoacán, Mexico. J S Am Earth Sci 93:439–448
Bronk Ramsey C (2009) Bayesian analysis of radiocarbon dates. Radiocarbon 51:337–360
Cai S, Tauxe L, Deng C, Pan Y, Jin G, Zheng J, Xie F, Qin H, Zhu R (2014) Geomagnetic intensity variations for the past 8 kyr: new archaeointensity results from eastern China. Earth Planet Sci Lett 392:217–229
Cai S, Chen W, Tauxe L, Deng C, Qin H, Pan Y, Zhu R (2015) New constraints on the variation of the geomagnetic field during the late Neolithic period: archaeointensity results from Sichuan, southwestern China. J Geophys Res 120:2056–2069
Cai S, Jin G, Tauxe L, Deng C, Qin H, Pan Y, Zhu R (2017) Archaeointensity results spanning the past 6 kiloyears from eastern China and implications for extreme behaviors of the geomagnetic field. Proc Natl Acad Sci 114:39–44
Coe RS (1967) Paleo-intensities of the Earth's magnetic field determined from tertiary and quaternary rocks. J Geophys Res 72:3247–3262
Fisher R (1953) Dispersion on a sphere. Proc R Soc Lond 217(Series A):295–305
Guérin G, Mercier N, Adamiec G (2011) Dose-rate conversion factors: update. Anc TL 29:5–8
Hatakeyama T, Shibuya H (2012) Geomagnetic secular variation in Japan from archeomagnetic data. In: Japan geoscience union meeting 2012 Abstract, STT58-01
Hayakawa Y (1995) Characteristics of Japanese loam, and its Eolian origin. Bull Volcanol Soc Japan 40:177–190 **(in Japanese with English abstract)**

Hong H, Yu Y, Lee CH, Kim RH, Park J, Doh SJ, Kim W, Sung H (2013) Globally strong geomagnetic field intensity circa 3000 years ago. Earth Planet Sci Lett 383:142–152
Kawachi S (1974) Geology of the Tateshinayama district, with Geological sheet map at 1:50,000. Geol Surv Japan, Tokyo, pp 119 **(in Japanese with English abstract)**
Kawachi S, Nakaya S, Muraki K (1978) YPm-IV pumice bed in Northern Yatsugatake, Yatsugatake Volcanic Chain, central Japan—studies on Yatsugatake tephra Part I. Bull Geol Surv Japan 29:21–33
Kharfi F, Boudraa L, Benabdelghani I, Bououden M (2019) TL dating and XRF clay provenance analysis of ancient brick at Cuicul Roman city, Algeria. J Radioanal Nucl Chem 320:395–403
Kirschvink JL (1980) The least-square line and plane and the analysis of paleomagnetic data. Geophys J R Astron Soc 62:699–718
Kondopoulou D, Aidona E, Ioannidis N, Polymeris GS, Tsolakis S (2015) Archaeomagnetic study and thermoluminescence dating of Protobyzantine kilns (Megali Kypsa, North Greece). J Archaeol Sci Rep 2:156–168
Leonhardt R, Heunemann C, Krása D (2004) Analyzing absolute paleointensity determinations: acceptance criteria and the software ThellierTool4.0. Geochem Geophys Geosyst 12:Q12016
May V, Chivas A, Dosseto A, Honda M, Matchan E, Phillips D, Price D (2018) Quaternary volcanic evolution in the continental backarc of southern Mendoza, Argentina. J S Am Earth Sci 84:88–103
McFadden PL (1982) Rejection of palaeomagnetic observations. Earth Planet Sci Lett 61:392–395
Nagata T, Arai T, Momose K (1963) Secular variation of the geomagnetic total force during the last 5000 years. J Geophys Res 68:5277–5281
Nakamura M (1991) A petrologic model for the younger period of Northern Yatsugatake Volcanoes, Central Japan. Bull Volcanol Soc Jpn 36:93–112 **(in Japanese with English abstract)**
Nishiki K, Matsumoto A, Uto K, Takahashi K, Miyake Y (2007) Reexamination of volcanic activity of Yatsugatake area, central Japan. J Geol Soc Japan 113:193–211 **(in Japanese with English abstract)**
Nishiki K, Takahashi K, Matsumoto A, Miyake Y (2011) Quaternary volcanism and tectonic history of the Suwa-Yatsugatake Volcanic Province, Central Japan. J Volcanol Geotherm Res 203:158–167
Oba T, Kawachi S (1997) The eruption stage of YPm-IV pumice in Mt. Yokodake, northern Yatsugatake volcanic group, estimated by petrochemistry and mineralogy. In: Japan earth planet sci joint meeting 1997 abstract, G31-06 **(in Japanese)**
Ogawa Y, Aoyama H, Yamamoto M, Tsutsui T, Terada A, Ohkura T, Kanda W, Koyama T, Kaneko T, Ohminato T, Ishizaki Y, Yoshimoto M, Ishimine Y, Nogami K, Mori T, Kikawada Y, Kataoka KS, Matsumoto T, Kamiishi I, Yamaguchi S, Ito Y, Tsunematsu K (2018) Comprehensive Survey of 2018 Kusatsu–Shirane Eruption. In: Proc symp on the natural disaster sciences, vol 55, pp 25–30 **(in Japanese)**
Oishi M (2015) ^{14}C dating of the Yt-Pm4 tephra, the youngest pumice fall from the Yatsugatake Volcano, Japan. Bull Volcanol Soc Jpn 60:477–481 **(in Japanese with English abstract)**
Oishi M, Suzuki T (2004) Tephrostratigraphy and eruptive history of the younger tephra beds from the Yatsugatake Volcano, central Japan. Bull Volcanol Soc Jpn 49:1–12 **(in Japanese with English abstract)**
Okuno M (1995) Eruption age inferred from radiocarbon accelerator (AMS) dating of paleosol. In: Summaries of researches using AMS, Nagoya University 6, pp 43–53 **(in Japanese with English abstract)**
Okuno M, Kobayashi T (2010) The latest magmatic eruption of Yokodake lava dome, Northern Yatsugatake Volcanoes, central Japan. In: Japanese geomorphological union 2010 abstract, O 22 **(in Japanese)**
Ono K (1990) Long-term forecast of volcanic eruptions. Bull Volcanol Soc Jpn 34:S201–S204 **(in Japanese)**
Paterson GA, Tauxe L, Biggin AJ, Shaar R, Jonestrask LC (2014) On improving the selection of Thellier-type paleointensity data. Geochem Geophys Geosyst 15:1180–1192
Pérez-Rodríguez N, Morales J, Goguitchaichvili A, García-Tenorio F (2019) A comprehensive paleomagnetic study from the last Plinian eruptions of Popocatepetl volcano: absolute chronology of lavas and estimation of emplacement temperatures of PDCs. Earth Planets Space 71:80. https://doi.org/10.1186/s40623-019-1059-x
Prescott JR, Hutton JT (1994) Cosmic ray contributions to dose rates for luminescence and ESR dating: large depths and long-term time variations. Radiat Meas 23(2–3):497–500
Rees-Jones J (1995) Optical dating of young sediments using fine-grained quartz. Anc TL 13:9–14
Reimer PJ, Bard E, Bayliss A, Beck JW, Blackwell PG, Bronk Ramsey C, Buck CE, Cheng H, Edwards RL, Friedrich M, Grootes PM, Guilderson TP, Haflidason H, Hajdas I, Hatté C, Heaton TJ, Hoffmann DL, Hogg AG, Hughen KA, Kaiser KF, Kromer B, Manning SW, Niu M, Reimer RW, Richards DA, Scott EM, Southon JR, Staff RA, Turney CSM, van der Plicht J (2013) IntCal13 and Marine13 radiocarbon age calibration curves 0–50,000 years cal BP. Radiocarbon 55:1869–1887
Risica G, Speranza F, Giordano G, De Astis G, Lucchi F (2019) Paleomagnetic dating of the Neostromboli succession. J Volcanol Geotherm Res 371:229–244
Sears DWG, Sears H, Sehlke A, Hughes SS (2018) Induced thermoluminescence as a method for dating recent volcanism: Hawaii County, Hawaii, USA. J Volcanol Geotherm Res 349:74–82
Shitaoka Y, Nagatomo T, Obata N (2009) Age determination of Ontake Pm1 pumice fall deposit (On-Pm1) by thermoluminescence method. Quat Res 48:295–300 **(in Japanese)**
Shitaoka Y, Hatano S, Tanabe K, Mori Y, Aoki S, Sakae O (2015) A new system for luminescence measurement and calibration of X-ray tube. Bull Geo-Environ Sci 17:107–110 **(in Japanese)**
Shitaoka Y, Saito T, Yamamoto J, Miyoshi M, Ishibashi H, Soda T (2019) Eruption age of Kannabe volcano using multi-dating: implications for age determination of young basaltic lava flow. Geochronometria 46:49–56
Tauxe L, Staudigel H (2004) Strength of the geomagnetic field in the cretaceous normal superchron: new data from submarine basaltic glass of the Troodos ophiolite. Geochem Geophys Geosyst 5(2):Q08H13
Yu Y (2012) High-fidelity paleointensity determination from historic volcanoes in Japan. J Geophys Res 117:B08101
Yu Y, Tauxe L, Genevey A (2004) Toward an optimal geomagnetic field intensity determination technique. Geochem Geophys Geosyst 5(2):Q02H07
Zijderveld JDA (1967) A.C. demagnetization of rocks: analysis of results. In: Collinson DW, Creer KM, Runcorn SK (eds) Methods in palaeomagnetism. Elsevier, Amsterdam, pp 254–286

Publisher's Note